Nano Research
2021, 14(10): 3497–3501
ISSN 1998-0124 CN 11-5974/O4
https://doi.org/10.1007/s12274-021-3639-x

Research Article

Intimate atomic Cu-Ag interfaces for high CO_2RR selectivity towards CH_4 at low over potential

Chungseok Choi[1,§], Jin Cai[1,§], Changsoo Lee[1,2,3,§], Hyuck Mo Lee[3], Mingjie Xu[4,5], and Yu Huang[1] (✉)

[1] *Department of Materials Science and Engineering, University of California, Los Angeles, CA 90095, USA*
[2] *Hydrogen Energy Department, Korea Institute of Energy Research, 152 Gajeong-ro, Yuseong-gu, Daejeon 34129, Republic of Korea*
[3] *Department of Materials Science and Engineering, Korea Advanced Institute of Science and Technology, 291 Daehak-ro, Yuseong-gu, Daejeon 34141, Republic of Korea*
[4] *Irvine Materials Research Institute (IMRI), University of California, Irvine, CA 92697, USA*
[5] *Department of Materials Science and Engineering, University of California, Irvine, CA 92697, USA*
[§] *Chungseok Choi, Jin Cai, and Changsoo Lee contributed equally to this work.*

Received: 10 March 2021 / **Revised:** 25 May 2021 / **Accepted:** 2 June 2021

ABSTRACT

Developing highly efficient electrochemical catalysts for carbon dioxide reduction reaction (CO_2RR) provides a solution to battle global warming issues resulting from ever-increasing carbon footprint due to human activities. Copper (Cu) is known for its efficiency in CO_2RR towards value-added hydrocarbons; hence its unique structural properties along with various Cu alloys have been extensively explored in the past decade. Here, we demonstrate a two-step approach to achieve intimate atomic Cu-Ag interfaces on the surface of Cu nanowires, which show greatly improved CO_2RR selectivity towards methane (CH_4). The specially designed Cu-Ag interfaces showed an impressive maximum Faradaic efficiency (FE) of 72% towards CH_4 production at −1.17 V (vs. reversible hydrogen electrode (RHE)).

KEYWORDS

electrochemical CO_2 reduction reaction, catalyst, copper, silver, bimetallic interface

1 Introduction

Humanity is at the brink of fossil fuel exhaustion and faces challenges of global climate change. Carbon dioxide (CO_2) emission is a primary driver of global warming and the reducing pH levels of the ocean. Meanwhile fossil fuels are not renewable and will eventually deplete. Creating a closed-loop process to recycle CO_2 to value-added fuels is a promising option to mitigate global warming and grant inexhaustible energy sources [1–4]. Developing efficient electrochemical catalysts for CO_2 reduction reaction (CO_2RR) is a prerequisite for establishing a carbon recycle loop and renewable energy technologies.

In the past decade, electrochemical CO_2RR has remarked prominent achievements in both scientific apprehension and technological developments. Among many electrocatalysts, copper (Cu) is the only known electrochemical catalyst to convert CO_2 to alternative energy fuels and hydrocarbons (especially methane (CH_4)) with sufficient current density and selectivity [5]. However, a mixture of primary products, competition with hydrogen evolution reaction (HER), and required high overpotential for CO_2RR on monometallic Cu still poses challenges. Therefore, designing Cu-based catalysts with high selectivity at low overpotentials is of great interest [6].

The prior art of research has improved Cu catalyst's modulation of structure defects [7–10], shapes [11–13], size [14], and chemical states [15–20] of Cu. For example, grain boundaries (GBs) exhibited ~ 2.5 times higher CO_2RR activity with less competitive reaction (HER) [21]. Cheng et al. reported that Cu's surface steps, having a combination of one strong and one weak CO binding site, enhance C_2 productions with reduced formation energy of the rate determining step (*OCCOH) to 0.52 eV [22]. Alloying Cu with a second metal is another attractive way to design catalysts [23]. However, Cu usually lost its extraordinary CO_2RR capability of producing hydrocarbon and oxygenates, having C_2 and C_3 carbons by forming an alloy with other elements [24–27]. Thus, interface Cu with neighboring unmixable second elements has been proposed to design Cu-based catalysts to retain the Cu's unique CO_2RR capability [27, 28]. Because of this complexity, the research in CuM (M denotes another metal element) alloy catalysts for electrochemical CO_2RR has not been sufficiently explored or compared with pure Cu. Silver (Ag) is a promising candidate to achieve such an unmixable Cu-M interface design because Ag and Cu are known for their thermodynamical immiscibility over all compositions at room temperature [29–34]. For example, Huang et al. reported that the interface between Cu catalysts and Ag catalysts was the crucial active site to enhance CO_2RR over pure Cu catalysts [34]. However, the interface between Cu and Ag has been limited because the boundary was miserly obtained between Cu and Ag catalysts. Maximizing the Cu and Ag interfaces at the atomic level is highly desired but challenging.

Herein, we report a two-step approach to build the interface

Address correspondence to yhuang@seas.ucla.edu

between Cu and Ag at the atomic level (Fig. 1). Cu nanowires (CuNWs) were first synthesized and followed by galvanic replacement from Cu to Ag to achieve *in situ* formation of CuAg ensembles, which builds CuNWs with rich Cu-Ag interfaces. The attractive Cu-Ag interfaces showed a dramatic change in CO_2RR selectivity from C_2H_4 to CH_4, which remarked a 63.29% ± 4.85% FE_{CH_4} (FE means Faradaic efficiency) at −1.12 ± 0.01 V (vs. reversible hydrogen electrode (RHE), referenced to all potentials) and an impressive maximum FE_{CH_4} of 72% at low potential of −1.17 V

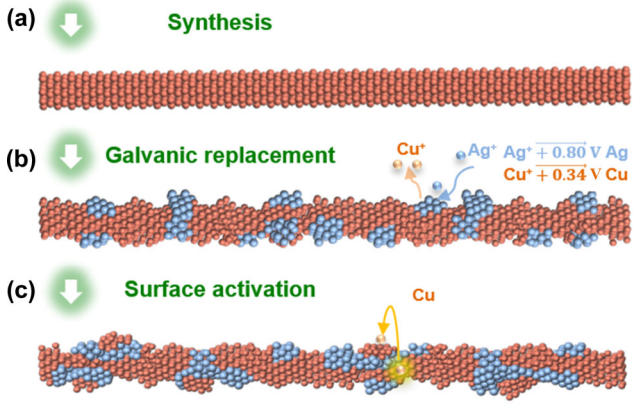

Figure 1 Schematic of preparing CuAgNWs. (a) The pure CuNWs are synthesized. (b) Galvanic replacement is conducted to partially replace Cu surface to Ag surface. (c) Atomic interfaces between Cu and Ag are further generated through *in situ* formation of CuAg ensembles during the electrochemical CO_2RR.

2 Results

We synthesized bimetallic CuAg nanowires (CuAgNWs) through a synthesis of CuNWs followed by galvanic replacement of Cu to Ag (Figs. 1(a) and 1(b)). To be specific, 22 mg of $CuCl_2{\cdot}2H_2O$, 50 mg of glucose, and 180 mg of hexadecylamine (HDA) were mixed in 10 mL of deionized (DI) water (18.2 MΩ/cm) under sonication for 15 min, then heated at 100 °C for 8 h in an oil bath. After the reaction solution cooled down to room temperature, 1.21 mg of $AgCH_3CO_2$ and 0.84 mg of imidazole were added to the CuNW solution, which was kept at 50 °C for 25 or 60 min without stirring for galvanic replacements from Cu to Ag. The relatively high standard reduction potential of Ag (($Ag^+ + e^- \rightarrow Ag(s)$, $E° = 0.80$ V) (standard hydrogen electrode)) compared to Cu (($Cu^{2+} + 2e^- \rightarrow Cu(s)$, $E° = 0.34$ V (standard hydrogen electrode)) [35] drives replacements from Cu to Ag on the surface of CuNWs. The synthesized CuAgNWs were washed five times with hexane/ethanol mixture and were collected by centrifuge. The CuAgNWs were characterized by transmission electron microscopy (TEM), Cs-corrected high-angle annular dark-field imaging scanning transmission electron microscope (HAADF STEM), energy-dispersive X-ray spectroscopy (EDX), and powder X-ray diffraction (PXRD). The average size of CuNWs (25 ± 7.7 nm) was obtained by averaging more than 100 NWs in width (Fig. S1 in the Electronic Supplementary Material (ESM)). Imidazole, a small molecular capping agent, was pivotal in slowing down the fast Ag galvanic replacement reaction on the surface of CuNWs and keeping one-dimensional structure of CuAgNWs without disintegrating into CuAg nanoparticles (NPs) (Fig. S2 in the ESM). The pure CuNWs showed flat and clean surfaces, whereas the uneven surface was observed after the Ag galvanic replacement on the surface of CuNWs (Fig. S3 in the ESM).

The PXRD peaks of CuAgNWs indicate no Bragg angle shift of Cu{111} and Ag{111} after the galvanic replacement of Ag for 25 min (Fig. 2), which indicates an unmixable pure Cu and Ag phase system without forming the CuAg alloy. High intensity of Ag{111} plane in CuAgNWs with the galvanic replacement for 60 min illustrates more replacements from Cu to Ag element for longer galvanic reaction times.

To quantify the bulk and surface composition of CuAgNWs, we carried out inductively coupled plasma atomic emission spectroscopy (ICP-AES) and X-ray photoelectron spectroscopy (XPS). Table 1 shows a summary of ICP and XPS composition analyses. The bulk composition from ICP analysis showed 82% of Cu and 18% of Ag (Cu8.2Ag1.8NWs) in CuAgNWs with the galvanic replacement for 60 min; and 90% of Cu and 10% of Ag (Cu9Ag1NWs) with the galvanic replacement for 25 min. In the case of XPS, the calculated electron inelastic mean free path of Cu at 992.3 eV and Ag at 365 eV are 1.67 and 0.727 nm, respectively [36], which reveals a surface limited component analysis of XPS for Cu and Ag metal. XPS analysis of Cu8.2Ag1.8NWs (60 min) illustrates two times higher Ag concentration than the ICP analysis, indicating richer Ag concentration on the surface of Cu8.2Ag1.8NWs. While, Cu9Ag1 which is synthesized from 25 min galvanic replacements shows comparable Ag concentration at bulk and surface of Cu9Ag1NWs, indicating that the galvanic replacement only occurs at the CuNW surface and Ag mainly stays near the surface.

Indeed Cs-corrected HAADF STEM images of CuNWs and EDX maps of the Cu9Ag1NWs confirmed that galvanic replacement of Cu to Ag on the surface (Fig. S4 in the ESM). The EDX maps showed Ag mainly located on the surface of CuNWs, and formed separate Ag phases from Cu phases in Cu9Ag1NWs (Figs. S4(c) and S4(d) in the ESM). Cu K and Ag L EDX maps illustrated that a thin layer of Ag covers the surface of CuNWs (Figs. S4(e) and S4(h) in the ESM). However, with longer (60 min) galvanic replacement, the Cu8.2Ag1.8NWs showed more uneven surfaces and much thicker surface coverage of Ag compared to Cu9Ag1NWs (25 min galvanic reaction) as shown in Fig. S5 in the ESM.

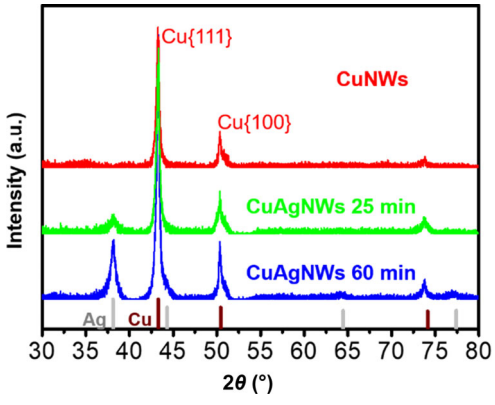

Figure 2 PXRD of CuNWs and bimetallic CuAgNWs after the galvanic replacement for 25 and 60 min (red_pure CuNWs, green_CuAgNWs after 25 min galvanic replacement, and blue_CuAgNWs after 60 min galvanic replacement).

Table 1 The atomic composition of CuNWs and CuAgNWs by ICP and XPS

Min.	Notation	ICP measurement		XPS measurement	
		Cu (at.%)	Ag (at.%)	Cu (at.%)	Ag (at.%)
0 min	Cu	100	0	100	0
25 min	Cu9Ag1	90.39 ± 6.03	9.611 ± 6.03	89.08 ± 3.37	10.93 ± 3.38
60 min	Cu8.2Ag1.8	82.11 ± 2.95	17.89 ± 2.95	68.13 ± 3.65	31.87 ± 3.65

We further found that electrochemical treatment of the as-prepared Cu9Ag1NWs can drive Cu to the surface of Cu9Ag1NWs and generate atomic Cu-Ag interfaces with more exposed Cu surface. The Cu9Ag1NW catalysts inks were prepared by mixing 4 mg of the CuAgNWs in 1 mL ethanol and 10 μL of 5% Nafion 117. We dropped 10 μL catalyst inks on the 1 cm diameter glassy carbon electrode. Subsequently, by using a high reduction bias (V = −1.05 V), we activated the CuAgNWs in CO_2-saturated 0.1 M $KHCO_3$ solution for 2 h. After such treatment, Fig. 3 showed the generated atomic Cu-Ag interfaces on the surface of Cu9Ag1NWs. EDX maps showed that Cu rose above the top of Ag-covered surface of as-prepared Cu9Ag1 NWs (Figs. 3(a) and 3(d), and Fig. S6 in the ESM). The interfaces between Cu ensembles and Ag layers were quite prominent in EDX maps of Cu component in Figs. 3(b) and 3(e), and Ag component in Figs. 3(c) and 3(f).

The migration of Cu atoms outward to the surface of the NWs can be understood based on the differential binding strengths of Cu and Ag to CO_2RR intermediates or products. Back et al. [37] reported that Cu(211) has −0.77 eV of CO binding energy (E_B[CO]), −0.16 eV of H binding energy (E_B[H]), and −0.07 eV of OH binding (E_B[OH]), which are all stronger than Ag(211) (−0.15 eV of E_B[CO], 0.30 eV of E_B[H], and 0.56 eV of OH binding E_B[OH]). Zhong et al. [38] also reported that the Cu has stronger E_B[H] and E_B[CO] than Ag. The Cu under Ag surface could go to the top surface because of Cu's stronger binding energies with hydrogen, carbon monoxide, and hydroxide compared with Ag. To confirm the molecules' types for the generation of the unique Cu-Ag surface ensembles structures, we carried out the activation process by changing purging gas of CO_2, CO, and H_2 at −1.05 V (vs. RHE) for 30 min, respectively. Figure S7 in the ESM illustrates that the Cu component went to the top surface at all purging conditions. Interestingly, in the Cu8.2Ag1.8NWs, the Cu and Ag elements separated into Cu particles and Ag straw structures (Fig. S8 in the ESM). This indicates a thick enough Ag surface layer might limit the movement of Cu towards the surface to rise above the Ag surface.

We conducted CO_2RR with CO_2-saturated 0.1 M $KHCO_3$ (pH 6.8) in a gas-tight H-cell at room temperature under atmospheric pressure. We analyzed effluent gas/liquid products at different applied potentials between −1.02 and −1.25 V (vs. RHE). To compare the CO_2RR performance of pure Ag, we also synthesized and conducted CO_2RR test of AgNPs (Fig. S9 in the ESM).

It is found that with increasing Ag content in the CuAgNWs, the electrochemically active surface area (ECSA) normalized current densities decreased (Fig. S10 in the ESM). Because liquid products from CO_2RR of these catalysts were less than 10%, we focused the discussion of Faradaic efficiency on gas-phase products (Fig. 4 and Tables S1–S3 in the ESM). Figure 4 shows FEs of CuNWs (Fig. 4(a)), Cu9Ag1NWs (Fig. 4(b)), Cu8.2Ag1.8NWs (Fig. 4(c)), and AgNPs (Fig. 4(d)). The pure CuNWs exhibited high selectivity of 60.37% ± 4.46% of $FE_{C_2H_4}$ at −1.06 V (vs. RHE), and 55.01% ± 7.58% of FE_{CH_4} at −1.23 V (vs. RHE) (Fig. 4(a)). However, Cu9Ag1NWs showed very different product selectivity. Cu9Ag1NWs suppressed C_2H_4 productions to less than ~ 21% at all measured potentials (Fig. 4(b)). At the same time, the CH_4 production from Cu9Ag1NWs started to rise at ~ −1.12 V (vs. RHE) with FE_{CH_4} 63.29% ± 4.85%, which continued to rise to an impressive maximum FE_{CH_4} 72% at low potential of −1.17 V, and maintained at 66.36% ± 4.18% of FE_{CH_4} at −1.20 V (Fig. 4(b)). Importantly, Cu9Ag1NWs remarkably retrenched −0.13 V applied potential to produce 60% FE_{CH_4} compared with CuNWs (Fig. S11 in the ESM).

The reaction pathways of CH_4 and C_2H_4 share a common *COH intermediate, which deviates to CH_4 with *HCOH and C_2H_4 with *OC-COH (*active sites of catalysts) [39]. Thus, catalyst's availability to adsorb H (H_{ad}) compared to adsorb CO (CO_{ad}) induces higher CH_4 selectivity over C_2H_4 selectivity. Chen et al. reported that hydrogen binding energy increases by ~ 1 eV/V while the CO binding energy varies little with applied potentials [39]. Assuming dominant hydrogen coverage at more negative than −0.8 V (vs. RHE) [39], at −1.12 V (vs. RHE) on the surface of CuAgNWs, the Cu portion would be covered by hydrogen (Cu-H*) while the surface of Ag was still dominant by CO (Ag-CO*). CO dominance on Ag surface was consistent with our observation of FE_{CO} over 90% at ~ −1.13 V (vs. RHE) on AgNPs (Fig. 4(d)). On CuAgNWs, the diffusion of CO from Ag section to the Cu section is likely more efficient due to the short diffusion length. Thus, efficient feeding of CO to hydrogen-covered Cu surface could make it favorable to generate *COH, and the dominant hydrogen coverage on the Cu surface might drive *COH to *HCOH and finally CH_4.

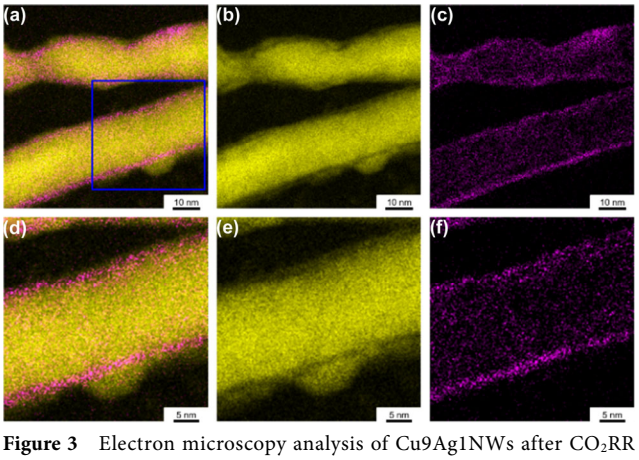

Figure 3 Electron microscopy analysis of Cu9Ag1NWs after CO_2RR at −1.05 V (vs. RHE) for 2 h. (a) EDX mapping of Cu K and Ag L on Cu9Ag1NWs. (b) Cu component and (c) Ag component in the EDX image of Cu9Ag1NWs. (d) EDX mapping of a Cu ensemble with Ag on the surface of Cu9Ag1NWs (zoom in the blue square in (a)). (e) Cu component and (f) Ag component in the EDX image of Cu and Ag ensemble on the surface of Cu9Ag1NWs. Yellow indicates Cu, and purple indicates Ag.

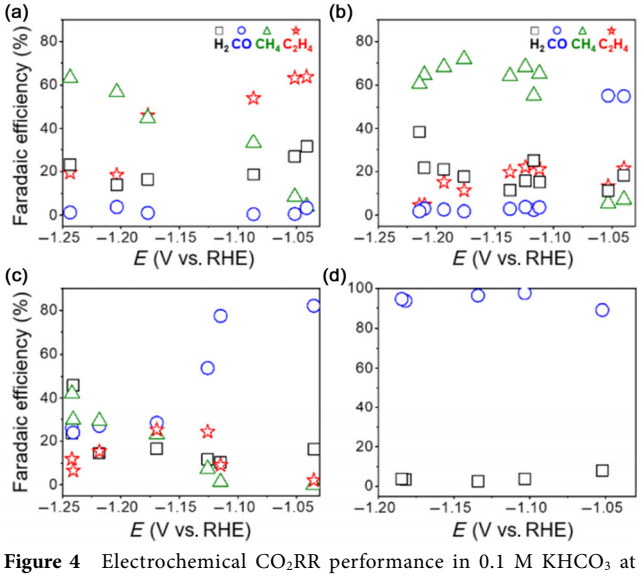

Figure 4 Electrochemical CO_2RR performance in 0.1 M $KHCO_3$ at room temperature and atmosphere pressure: (a) FEs of CuNWs, (b) FEs of Cu9Ag1NWs, (c) FEs of Cu8.2Ag1.8NWs, and (d) FEs of AgNPs.

To further investigate the importance of the different interfaces between Cu and Ag components for high CH_4 generation, we compared FEs of Cu9Ag1NWs and Cu8.2Ag1.8NWs. Both Cu9Ag1NWs and Cu8.2Ag1.8NWs showed higher selectivity of CO (> 60% FE_{CO}) at ~ −1.05 V (vs. RHE) than pure CuNWs (Figs. 4(a)–4(c)), confirming *CO contribution from the Ag component. However, the Cu8.2Ag1.8NWs still showed high CO selectivity (53.21% ± 20.00%) with low CH_4 production (10.55% ± 9.15%) at −1.13% ± 0.02% V (vs. RHE) (Tables S1 and S2 in the ESM), while Cu9Ag1NWs already demonstrated over 60% FE_{CH_4}. HRTEM and EDX showed larger separations between Cu and Ag components in Cu8.2Ag1.8NWs (Fig. S8 in the ESM) than Cu9Ag1NWs (Fig. S3 in the ESM).

This indicates that an intimate atomic level Cu-Ag interface between the Cu and Ag components is necessary to promote the synergistic effect of CO-Ag* and H-Cu* for high CH_4 selectivity. To the best of our knowledge, the Cu9Ag1NWs provide the highest FE_{CH_4} at the lowest applied potential 72% of FE_{CH_4} at −1.17 V (vs. RHE) in H-cell with standard glassy carbon electrode at room temperature and atmospheric pressure (0.1 M $KHCO_3$) compared to all other materials reported in the literature to date (Table 2).

Table 2 Summary of CO_2RR to CH_4 production on all other materials

Catalyst	Applied potentials *V* (vs. RHE)	Max. FE_{CH_4}	Electrolyte	Cell	Source
Cu9Ag1NWs	−1.17	72%	0.1 M $KHCO_3$	H-cell	This work
CuNWs	−1.25	55%	0.1 M $KHCO_3$	H-cell	[40]
Single atom Cu on CeO_2	−1.8	58%	0.1 M $KHCO_3$	H-cell	[41]
Cu electrode	~ −1.2	62%	0.1 M $KHCO_3$	H-cell	[42]
CRD-Cu_3Pd	−1.2	40.6%	0.1 M $KHCO_3$	H-cell	[43]
Cu/CeO_{2-x}	−1.2	54%	0.1 M $KHCO_3$	H-cell	[44]
Cu_2O@CuHHTP	−1.4	73%	0.1 M $KHCO_3$	H-cell	[45]
La_2CuO_4	−1.4	56.3%	0.1 M $KHCO_3$	H-cell	[46]

3 Conclusion

We successfully generated atomic Cu-Ag ensembles via *ex-situ* galvanic replacement from Cu to Ag, followed by an *in-situ* electrochemical activation approach. The atomic Cu-Ag ensemble interfaces showed a change of CO_2RR selectivity from C_2H_4 to CH_4, which remarked the highest FE_{CH_4} at the lowest applied potential 72% of FE_{CH_4} at −1.17 V (vs. RHE) in H-cell. These findings suggest an effective way to generate unmixable atomic ensemble Cu-Ag interfaces to enhance CH_4 selectivity with lower over potential under operando conditions. This approach can be expanded to other unmixable metal atoms to engineer the atomic ensemble interfaces for desired catalytic properties.

Acknowledgements

TEM work was conducted using the facilities in the electron imaging center of California NanoSystems Institute at the University of California Los Angles and the Irvine Materials Research Institute at the University of California Irvine. C. C., J. C. and Y. H. acknowledge support by the Office of Naval Research (ONR) (No. N000141712608). C. S. L. and H. M. L. acknowledge support by a National Research Foundation (NRF) of Korea grant funded by the Korean Government (Nos. NRF-2017 R1E1A1A03071049 and NRF-2020R1A5A6017701).

Electronic Supplementary Material: Supplementary material (further details of the synthesis process, TEM image, materials and electrical measurements) is available in the online version of this article at https://doi.org/10.1007/s122741-3639-x.

References

[1] Schreier, M.; Héroguel, F.; Steier, L.; Ahmad, S.; Luterbacher, J. S.; Mayer, M. T.; Luo, J. S.; Grätzel, M. Solar conversion of CO_2 to CO using Earth-abundant electrocatalysts prepared by atomic layer modification of CuO. *Nat. Energy* **2017**, *2*, 17087.

[2] Lin, S.; Diercks, C. S.; Zhang, Y. B.; Kornienko, N.; Nichols, E. M.; Zhao, Y. B.; Paris, A. R.; Kim, D.; Yang, P. D.; Yaghi, O. M. Covalent organic frameworks comprising cobalt porphyrins for catalytic CO_2 reduction in water. *Science* **2015**, *349*, 1208–1213.

[3] Gao, S.; Lin, Y.; Jiao, X. C.; Sun, Y. F.; Luo, Q. Q.; Zhang, W. H.; Li, D. Q.; Yang, J. L.; Xie, Y. Partially oxidized atomic cobalt layers for carbon dioxide electroreduction to liquid fuel. *Nature* **2016**, *529*, 68–71.

[4] Dinh, C. T.; Burdyny, T.; Kibria, G.; Seifitokaldani, A.; Gabardo, C. M.; De Arquer, F. P. G.; Kiani, A.; Edwards, J. P.; De Luna, P.; Bushuyev, O. S. et al. CO_2 electroreduction to ethylene via hydroxide-mediated copper catalysis at an abrupt interface. *Science* **2018**, *360*, 783–787.

[5] Yoshio, H.; Katsuhei, K.; Shin, S.; Production of CO and CH_4 in electrochemical reduction of CO_2 at metal electrodes in aqueous hydrogencarbonate solution. *Chem. Lett.* **1985**, *14*, 1695–1698.

[6] Cheng, T.; Xiao, H.; Goddard III, W. A. Reaction mechanisms for the electrochemical reduction of CO_2 to CO and formate on the Cu(100) surface at 298 K from quantum mechanics free energy calculations with explicit water. *J. Am. Chem. Soc.* **2016**, *138*, 13802–13805.

[7] Verdaguer-Casadevall, A.; Li, C. W.; Johansson, T. P.; Scott, S. B.; McKeown, J. T.; Kumar, M.; Stephens, I. E. L.; Kanan, M. W.; Chorkendorff, I. Probing the active surface sites for CO reduction on oxide-derived copper electrocatalysts. *J. Am. Chem. Soc.* **2015**, *137*, 9808–9811.

[8] Feng, X. F.; Jiang, K. L.; Fan, S. S.; Kanan, M. W. Grain-boundary-dependent CO_2 electroreduction activity. *J. Am. Chem. Soc.* **2015**, *137*, 4606–4609.

[9] Li, C. W.; Ciston, J.; Kanan, M. W. Electroreduction of carbon monoxide to liquid fuel on oxide-derived nanocrystalline copper. *Nature* **2014**, *508*, 504–507.

[10] Li, C. W.; Kanan, M. W. CO_2 reduction at low overpotential on Cu electrodes resulting from the reduction of thick Cu_2O films. *J. Am. Chem. Soc.* **2012**, *134*, 7231–7234.

[11] Ma, M.; Djanashvili, K.; Smith, W. A. Controllable hydrocarbon formation from the electrochemical reduction of CO_2 over Cu nanowire arrays. *Angew. Chem., Int. Ed.* **2016**, *55*, 6680–6684.
[12] Loiudice, A.; Lobaccaro, P.; Kamali, E. A.; Thao, T.; Huang, B. H.; Ager, J. W.; Buonsanti, R. Tailoring copper nanocrystals towards C_2 products in electrochemical CO_2 reduction. *Angew. Chem., Int. Ed.* **2016**, *55*, 5789–5792.
[13] Raciti, D.; Livi, K. J.; Wang, C. Highly dense Cu nanowires for low-overpotential CO_2 reduction. *Nano Lett.* **2015**, *15*, 6829–6835.
[14] Reske, R.; Mistry, H.; Behafarid, F.; Cuenya, B. R.; Strasser, P. Particle size effects in the catalytic electroreduction of CO_2 on Cu nanoparticles. *J. Am. Chem. Soc.* **2014**, *136*, 6978–6986.
[15] Mistry, H.; Varela, A. S.; Bonifacio, C. S.; Zegkinoglou, I.; Sinev, I.; Choi, Y. W.; Kisslinger, K.; Stach, E. A.; Yang, J. C.; Strasser, P. et al. Highly selective plasma-activated copper catalysts for carbon dioxide reduction to ethylene. *Nat. Commun.* **2016**, *7*, 12123.
[16] Lum, Y. W.; Ager, J. W. Stability of residual oxides in oxide-derived copper catalysts for electrochemical CO_2 reduction investigated with ^{18}O labeling. *Angew. Chem., Int. Ed.* **2018**, *57*, 551–554.
[17] Lum, Y. W.; Yue, B. B.; Lobaccaro, P.; Bell, A. T.; Ager, J. W. Optimizing C-C coupling on oxide-derived copper catalysts for electrochemical CO_2 reduction. *J. Phys. Chem. C* **2017**, *121*, 14191–14203.
[18] Gao, D. F.; Zhang, Y.; Zhou, Z. W.; Cai, F.; Zhao, X. F.; Huang, W. G.; Li, Y. S.; Zhu, J. F.; Liu, P.; Yang, F. et al. Enhancing CO_2 electroreduction with the metal-oxide interface. *J. Am. Chem. Soc.* **2017**, *139*, 5652–5655.
[19] Favaro, M.; Xiao, H.; Cheng, T.; Goddard III, W. A.; Yano, J.; Crumlin, E. J. Subsurface oxide plays a critical role in CO_2 activation by Cu(111) surfaces to form chemisorbed CO_2, the first step in reduction of CO_2. *Proc. Natl. Acad. Sci. USA* **2017**, *114*, 6706–6711.
[20] Xiao, H.; Goddard III, W. A.; Cheng, T.; Liu, Y. Y. Cu metal embedded in oxidized matrix catalyst to promote CO_2 activation and CO dimerization for electrochemical reduction of CO_2. *Proc. Natl. Acad. Sci. USA* **2017**, *114*, 6685–6688.
[21] Mariano, R. G.; McKelvey, K.; White, H. S.; Kanan, M. W. Selective increase in CO_2 electroreduction activity at grain-boundary surface terminations. *Science* **2017**, *358*, 1187–1191.
[22] Cheng, T.; Xiao, H.; Goddard III, W. A. Nature of the active sites for CO reduction on copper nanoparticles; suggestions for optimizing performance. *J. Am. Chem. Soc.* **2017**, *139*, 11642–11645.
[23] Hansen, H. A.; Shi, C.; Lausche, A. C.; Peterson, A. A.; Nørskov, J. K. Bifunctional alloys for the electroreduction of CO_2 and CO. *Phys. Chem. Chem. Phys.* **2016**, *18*, 9194–9201.
[24] Hahn, C.; Abram, D. N.; Hansen, H. A.; Hatsukade, T.; Jackson, A.; Johnson, N. C.; Hellstern, T. R.; Kuhl, K. P.; Cave, E. R.; Feaster, J. T. et al. Synthesis of thin film AuPd alloys and their investigation for electrocatalytic CO_2 reduction. *J. Mater. Chem. A* **2015**, *3*, 20185–20194.
[25] Ren, D.; Ang, B. S. H.; Yeo, B. S. Tuning the selectivity of carbon dioxide electroreduction toward ethanol on oxide-derived Cu_xZn catalysts. *ACS Catal.* **2016**, *6*, 8239–8247.
[26] Torelli, D. A.; Francis, S. A.; Crompton, J. C.; Javier, A.; Thompson, J. R.; Brunschwig, B. S.; Soriaga, M. P.; Lewis, N. S. Nickel-gallium-catalyzed electrochemical reduction of CO_2 to highly reduced products at low overpotentials. *ACS Catal.* **2016**, *6*, 2100–2104.
[27] Ma, S. C.; Sadakiyo, M.; Heim, M.; Luo, R.; Haasch, R. T.; Gold, J. I.; Yamauchi, M.; Kenis, P. J. A.; Electroreduction of carbon dioxide to hydrocarbons using bimetallic Cu-Pd catalysts with different mixing patterns. *J. Am. Chem. Soc.* **2017**, *139*, 47–50.
[28] Clark, E. L.; Hahn, C.; Jaramillo, T. F.; Bell, A. T. Electrochemical CO_2 reduction over compressively strained CuAg surface alloys with enhanced multi-carbon oxygenate selectivity. *J. Am. Chem. Soc.* **2017**, *139*, 15848–15857.
[29] Hatsukade, T.; Kuhl, K. P.; Cave, E. R.; Abram, D. N.; Jaramillo, T. F. Insights into the electrocatalytic reduction of CO_2 on metallic silver surfaces. *Phys. Chem. Chem. Phys.* **2014**, *16*, 13814–13819.
[30] Sanchez, J. M.; Stark, J. P.; Moruzzi, V. L. First-principles calculation of the Ag-Cu phase diagram. *Phys. Rev. B* **1991**, *44*, 5411–5418.
[31] Hoang, T. T. H.; Verma, S.; Ma, S. C.; Fister, T. T.; Timoshenko, J.; Frenkel, A. I.; Kenis, P. J. A.; Gewirth, A. A. Nanoporous copper silver alloys by additive-controlled electrodeposition for the selective electroreduction of CO_2 to ethylene and ethanol. *J. Am. Chem. Soc.* **2018**, *140*, 5791–5797.
[32] Lee, S.; Park, G.; Lee, J. Importance of Ag-Cu biphasic boundaries for selective electrochemical reduction of CO_2 to ethanol. *ACS Catal.* **2017**, *7*, 8594–8604.
[33] Wang, Y.; Wang, D. G.; Dares, C. J.; Marquard, S. L.; Sheridan, M. V.; Meyer, T. J.; CO_2 reduction to acetate in mixtures of ultrasmall $(Cu)_n$, $(Ag)_m$ bimetallic nanoparticles. *Proc. Natl. Acad. Sci. USA* **2018**, *115*, 278–283.
[34] Huang, J. F.; Mensi, M.; Oveisi, E.; Mantella, V.; Buonsanti, R. Structural sensitivities in bimetallic catalysts for electrochemical CO_2 reduction revealed by Ag-Cu nanodimers. *J. Am. Chem. Soc.* **2019**, *141*, 2490–2499.
[35] Reger, D. L.; Goode, S. R.; Mercer, E. E. *Chemistry, Principles & Practice*, 2nd ed.; Saunders College Pub., 1997.
[36] Shinotsuka, H.; Tanuma, S.; Powell, C. J.; Penn, D. R. Calculations of electron inelastic mean free paths. X. Data for 41 elemental solids over the 50 eV to 200 keV range with the relativistic full Penn algorithm. *Surf. Interface Anal.* **2015**, *47*, 871–888.
[37] Back, S.; Kim, H.; Jung, Y. Selective heterogeneous CO_2 electroreduction to methanol. *ACS Catal.* **2015**, *5*, 965–971.
[38] Zhong, M.; Tran, K.; Min, Y. M.; Wang, C. H.; Wang, Z. Y.; Dinh, C. T.; De Luna, P.; Yu, Z. Q.; Rasouli, A. S.; Brodersen, P. et al. Accelerated discovery of CO_2 electrocatalysts using active machine learning. *Nature* **2020**, *581*, 178–183.
[39] Cheng, T.; Xiao, H.; Goddard III, W. A. Full atomistic reaction mechanism with kinetics for CO reduction on Cu(100) from *ab initio* molecular dynamics free-energy calculations at 298 K. *Proc. Natl. Acad. Sci. USA* **2017**, *114*, 1795–1800.
[40] Li, Y. F.; Cui, F.; Ross, M. B.; Kim, D.; Sun, Y. C.; Yang, P. D. Structure-sensitive CO_2 electroreduction to hydrocarbons on ultrathin 5-fold twinned copper nanowires. *Nano Lett.* **2017**, *17*, 1312–13172.
[41] Wang, Y. F.; Chen, Z.; Han, P.; Du, Y. H.; Gu, Z. X.; Xu, X.; Zheng, G. F. Single-atomic Cu with multiple oxygen vacancies on ceria for electrocatalytic CO_2 reduction to CH_4. *ACS Catal.* **2018**, *8*, 7113–7119.
[42] Ren, D.; Fong, J. H.; Yeo, B. S. The effects of currents and potentials on the selectivities of copper toward carbon dioxide electroreduction. *Nat. Commun.* **2018**, *9*, 925.
[43] Zhu, W. J.; Zhang, L.; Yang, P. P.; Chang, X. X.; Dong, H.; Li, A.; Hu, C. L.; Huang, Z. Q.; Zhao, Z. J.; Gong, J. L. Morphological and compositional design of Pd–Cu bimetallic nanocatalysts with controllable product selectivity toward CO_2 electroreduction. *Small* **2018**, *14*, 1703314.
[44] Varandili, S. B.; Huang, J. F.; Oveisi, E.; De Gregorio, G. L.; Mensi, M.; Strach, M.; Vavra, J.; Gadiyar, C.; Bhowmik, A.; Buonsanti, R. Synthesis of Cu/CeO_{2-x} nanocrystalline heterodimers with interfacial active sites to promote CO_2 electroreduction. *ACS Catal.* **2019**, *9*, 5035–5046.
[45] Yi, J. D.; Xie, R. K.; Xie, Z. L.; Chai, G. L.; Liu, T. F.; Chen, R. P.; Huang, Y. B.; Cao, R. Highly selective CO_2 electroreduction to CH_4 by *in situ* generated Cu_2O single-type sites on a conductive MOF: Stabilizing key intermediates with hydrogen bonding. *Angew. Chem., Int. Ed.* **2020**, *59*, 23641–23648.
[46] Chen, S. H.; Su, Y. Q.; Deng, P. L.; Qi, R. J.; Zhu, J. X.; Chen, J. X.; Wang, Z. T.; Zhou, L.; Guo, X. P.; Xia, B. Y. Highly selective carbon dioxide electroreduction on structure-evolved copper perovskite oxide toward methane production. *ACS Catal.* **2020**, *10*, 4640–4646.